Interdisciplinary Information Sciences Vol. 25, No. 2 (2019) 147–160

ISSN 1340-9050 print/1347-6157 online
DOI 10.4036/iis.2019.B.02

Optimal Design by Adaptive Mesh Refinement on Shape Optimization of Flow Fields Considering Proper Orthogonal Decomposition

Takashi NAKAZAWA[1,*] and Chihiro NAKAJIMA[2]

[1]*Center for Mathematical Modeling and Data Science, Osaka University, Osaka 560-8531, Japan*
[2]*Graduate School of Information Sciences, Tohoku University, Sendai 980-8579, Japan*

This paper presents optimal design using Adaptive Mesh Refinement (AMR) with shape optimization method. The method suppresses time periodic flows driven only by the non-stationary boundary condition at a sufficiently low Reynolds number using Snapshot Proper Orthogonal Decomposition (Snapshot POD). For shape optimization, the eigenvalue in Snapshot POD is defined as a cost function. The main problems are non-stationary Navier–Stokes problems and eigenvalue problems of POD. An objective functional is described using Lagrange multipliers and finite element method. Two-dimensional cavity flow with a disk-shaped isolated body is adopted. The non-stationary boundary condition is defined on the top boundary and non-slip boundary condition respectively for the side and bottom boundaries and for the disk boundary. For numerical demonstration, the disk boundary is used as the design boundary. Using H^1 gradient method for domain deformation, all triangles over a mesh are deformed as the cost function decreases. To avoid decreasing the numerical accuracy based on squeezing triangles, AMR is applied throughout the shape optimization process to maintain numerical accuracy equal to that of a mesh in the initial domain. The combination of eigenvalues that can best suppress the time periodic flow is investigated.

KEYWORDS: Adaptive Mesh Refinement, adjoint method, cavity flow, proper orthogonal decomposition, shape optimization problem

1. Introduction

This paper presents solution of a shape optimization problem achieved using Adaptive Mesh Refinement (AMR) for suppressing a moderate time periodic flow. Recently, Nakazawa [1] specifically examined construction of a shape optimization method based on Snapshot Proper Orthogonal Decomposition (Snapshot POD). The method can suppress a time periodic flow at a sufficiently low Reynolds number. In an earlier study [1], AMR was not applied. It therefore remains unclear whether the cost function decreases sufficiently to take its minimum value, or not. Consequently, in this study, AMR is applied after the mesh is reshaped by the sensitivity at each reshaping step. Then the combination of eigenvalues which can best suppress the time periodic flow is investigated. The particular history, background, and procedure of the suggested shape optimization problem with AMR are described below.

With the rapid development of computer technology and numerical methods, shape optimization based on computational fluid dynamics (CFD) is playing an important role in fluid mechanics and aerodynamics design. Shape optimization problems in fluid dynamics were first addressed by O. Pironneau [2, 3] for the respective domains in which the stationary Stokes and Navier–Stokes equations are defined. Subsequently, J. Haslinger and R. A. Makinen [4], B. Mohammadi and O. Pironneau [5], and M. Moubachir and J. P. Zolesio [6] constructed fundamental frameworks of flow-field shape-optimization problems. Recently, many researchers are examining the topic [7–10]. Efficient but accurate numerical methods must be used for such flow computations within an optimization process. Nevertheless, controlling the associated complex fluid flow behavior is difficult when generating an efficient mesh before knowing the new solution in a shape optimization problem. Therefore, most shape optimization algorithms are based on a fixed computational mesh. A computational grid represents a compromise between accuracy and efficiency. A solution might be the use of AMR.

From finite element theory, meshes with equilateral triangles are well known to be more suitable for isotropic problems. However, the notion of equilaterality involves lengths through scalar products in a given metric. Therefore, anisotropic meshes might be regarded as isotropic with respect to a different metric. We can adapt the mesh to follow the solution if the metric is defined using *a posteriori* error estimation. An unstructured grid environment is the natural framework for the introduction of general adaptivity and the anisotopy concept. Castro-Diaz and Hecht [11] described

Received December 17, 2018; Accepted July 29, 2019; J-STAGE Advance published September 10, 2019
2010 Mathematics Subject Classification: Primary 65K10, Secondary 65K25.
This work is supported by JSPS KAKENHI (16K20906).
*Corresponding author. E-mail: nakazawa@sigmath.es.osaka-u.ac.jp

numerical procedures related to AMR with the metric. Alauzet *et al.* [12] presented its mathematical proof in continuous and discrete spaces of the domain. Castro-Diaz *et al.* [13], Mohammadi and Hecht [14], and Frey *et al.* [15] used it for flow-field shape optimization. The present study also applies it to the author-suggested shape optimization problem.

The original motivation is explained below. Although flow stabilization presents the important challenge of choosing which research field best addresses flow control, few reports of the relevant literature describe flow stabilization by shape optimization. Nakazawa [16] reported that minimization and maximization problems of dissipation energy are solved in two-dimensional cavity flow, where the stationary Navier–Stokes problem is used as the main problem and where the dissipation energy is used as the cost function. After shape optimization, linear stability analysis is conducted in the initial and the optimal domains. The critical Reynolds numbers are, respectively, decreasing and increasing. Next, for controlling flow stability more directly, Nakazawa and Azegami [17] reported a pioneering shape optimization method used to stabilize the disturbances. The method is based on linear stability theory. Particularly, the real part of the leading eigenvalue is used as the cost function. The stationary Navier–Stokes problem and the eigenvalue problem of the linear stability analysis are cited as main problems for obtaining the cost function. However, the methods explained above are not available for the case in which the non-stationary boundary condition is defined because the stationary Navier–Stokes problem should be solved as described in an earlier report [16].

To address the challenge explained above, the author constructed a shape optimization method [1] using Snapshot POD, in which the eigenvalue in Snapshot POD is defined as the cost function. A remarkable feature of this suggested shape optimization problem is that a time periodic flow driven solely by the non-stationary boundary condition at a sufficiently low Reynolds number is developed or suppressed efficiently. That is possible because the eigenvalue (cost function) shows the L^2 norm of the velocity vector, which takes the time average or the time fluctuation by decomposing the time periodic flow into primary components. A brief summary of the shape optimization problem is presented below.

The sum of eigenvalues in POD is defined as the cost function. For this study, the non-stationary Navier–Stokes problem and the eigenvalue problem in POD are used as the main problems. The main problems are transformed from strong forms to weak forms with trial functions based on a standard application of finite element method (FEM). The functional is described using Lagrange multipliers with FEM. Next, its first variation, which is the same as the material derivative, is derived to evaluate sensitivity using adjoint variable method. An initial domain is reshaped iteratively to obtain an optimal domain. Then the H^1 gradient method [18] is used for stable domain deformation. However, AMR is not applied. It is therefore unclear that the cost function is decreasing sufficiently to take the minimum value. Thereby, this paper uses AMR after the mesh is reshaped by the sensitivity, where the new mesh is generated with respect to the metric as constructed for an earlier study [11, 12]. Subsequently, the combination of eigenvalues which can most suppress the time periodic flow is investigated.

For numerical demonstrations with FreeFEM++ [19] for all numerical calculations, the same problem is addressed as explained below. Two-dimensional cavity flow with a disk-shaped isolated body is adopted. The non-stationary boundary condition is defined for the top boundary and non-slip boundary condition for the boundaries not only of the side and bottom, but also of the disk. The disk boundary is used as the design boundary. Therefore, the disk is reshaped by a shape optimization process as the cost function decreases, where the domain variation is obtained using sensitivity analysis and some cost functions combining eigenvalues with various primary components. After numerical calculations, the eigenvalues of Snapshot POD are compared in the initial domain and the optimal domain. Results confirm the effectiveness of using AMR for the suggested shape optimization problem. Mathematical aspects and specific details of such an optimization problem are explained elsewhere in the relevant literature [1].

2. Formulation of the Problem

2.1 Initial domain

Letting Ω_0 be a fixed bounded Lipschitz domain in $\mathbb{R}^d$ ($d \in \mathbb{N}$), and letting Ω be an open subset of Ω_0, with a position vector denoted as $\boldsymbol{x} \in \mathbb{R}^d$, then, as described herein, a two-dimensional cavity flow with a disk-shaped isolated body Ω is adopted as the initial domain. For $d = 2$, the initial domain is $\Omega \subset \Omega_0 \subset \mathbb{R}^2$ as

$$\Omega = \Omega_{\mathrm{M}} \backslash \bar{\Omega}_{\mathrm{m}}, \tag{2.1}$$

$$\Omega_{\mathrm{M}} = \{(x, y);\ 0 < x < 1,\ 0 < y < 1\}, \tag{2.2}$$

$$\Omega_{\mathrm{m}} = \{(x, y);\ |(x, y) - (0.5, 0.5)| < 0.1\}, \tag{2.3}$$

regarding the boundary as

$$\Gamma_{\mathrm{top}} = \{(x, y);\ 0 \leq x \leq 1,\ y = 1\}, \tag{2.4}$$

$$\Gamma_{\mathrm{wall}} = \partial\Omega_{\mathrm{M}} \backslash \Gamma_{\mathrm{top}}. \tag{2.5}$$

For domain reshaping, the boundary of the disk $\partial\Omega_{\mathrm{m}}$ is regarded as the design boundary.

2.2 Domain variation

We consider domain deformation $\boldsymbol{\phi}$ as $\Omega \to \boldsymbol{\phi}(\Omega)$, where $\boldsymbol{\phi}$ is $\mathbb{R}^d$-valued function. For $|\varepsilon| \ll 1$, mapping $\boldsymbol{\phi}$ is represented by $\boldsymbol{\phi} = \boldsymbol{\phi}_0 + \varepsilon\boldsymbol{\varphi}$ in $W^{1,\infty}(\Omega, \mathbb{R}^d)$. Then we designate it by the identity map $\boldsymbol{\phi}_0(\Omega) = \Omega$ and the domain variation $\boldsymbol{\varphi}$.

We assume ζ_1 as a scalar-valued function describing a physical state in Ω, and ζ_2 as its corresponding adjoint variables. For such $\zeta = \{\zeta_1, \zeta_2\}$, we introduce the following functional in Ω and $\boldsymbol{\phi}(\Omega)$:

$$L(\Omega, \zeta(\boldsymbol{x})) = \int_\Omega G(\boldsymbol{x}, \zeta(\boldsymbol{x}))\, dx, \tag{2.6}$$

$$L(\boldsymbol{\phi}(\Omega), \zeta(\boldsymbol{\phi}(\boldsymbol{x}))) = \int_{\boldsymbol{\phi}(\Omega)} G(\boldsymbol{\phi}(\boldsymbol{x}), \zeta(\boldsymbol{\phi}(\boldsymbol{x}))\boldsymbol{\phi}(dx), \tag{2.7}$$

where G represents a real-valued given energy function.

For domain deformation, the Jacobi matrices are written as

$$(\nabla\boldsymbol{\phi}^{\mathrm{T}})^{\mathrm{T}} = (\nabla\boldsymbol{\phi}_0^{\mathrm{T}})^{\mathrm{T}} + \varepsilon(\nabla\boldsymbol{\varphi}^{\mathrm{T}})^{\mathrm{T}} + o(\varepsilon^2). \tag{2.8}$$

The determinant is obtained as

$$\det((\nabla\boldsymbol{\phi}^{\mathrm{T}})^{\mathrm{T}}) = 1 + \varepsilon\nabla\cdot\boldsymbol{\varphi} + o(\varepsilon^2). \tag{2.9}$$

Therefore,

$$\begin{aligned}\boldsymbol{\phi}(dx) &= \det((\nabla\boldsymbol{\phi}^{\mathrm{T}})^{\mathrm{T}})\, dx \\ &= (1 + \varepsilon\nabla\cdot\boldsymbol{\varphi} + o(\varepsilon^2))\, dx.\end{aligned} \tag{2.10}$$

The density function $G(\boldsymbol{\phi}(\boldsymbol{x}), \zeta(\boldsymbol{\phi}(\boldsymbol{x}))$ in $\boldsymbol{\phi}(\Omega)$ is deduced as

$$\begin{aligned}G(\boldsymbol{\phi}(\boldsymbol{x}), \zeta(\boldsymbol{\phi}(\boldsymbol{x})) &= G(\boldsymbol{x}, \zeta(\boldsymbol{x})) + \varepsilon\dot{G}(\boldsymbol{x}, \zeta(\boldsymbol{x})) + o(\varepsilon^2) \\ &= G(\boldsymbol{x}, \zeta(\boldsymbol{x})) + \varepsilon(G'(\boldsymbol{x}, \zeta(\boldsymbol{x})) + \boldsymbol{\varphi}\cdot\nabla G(\boldsymbol{x}, \zeta(\boldsymbol{x}))) + o(\varepsilon^2).\end{aligned} \tag{2.11}$$

Next, from Eqs. (2.10) and (2.11), the functional in $\boldsymbol{\phi}(\Omega)$ can be rewritten as

$$\begin{aligned}L(\boldsymbol{\phi}(\Omega), \zeta(\boldsymbol{\phi}(\boldsymbol{x}))) &= \int_{\boldsymbol{\phi}(\Omega)} G(\boldsymbol{\phi}(\boldsymbol{x}), \zeta(\boldsymbol{\phi}(\boldsymbol{x}))\boldsymbol{\phi}(dx) \\ &= L(\Omega, \zeta(\boldsymbol{x})) + \varepsilon\int_\Omega \{G'(\boldsymbol{x}, \zeta(\boldsymbol{x})) + \boldsymbol{\varphi}\cdot\nabla G(\boldsymbol{x}, \zeta(\boldsymbol{x})) + G(\boldsymbol{x}, \zeta(\boldsymbol{x}))\nabla\cdot\boldsymbol{\varphi}\}\, dx + o(\varepsilon^2).\end{aligned} \tag{2.12}$$

The first variation of the functional is expressed as

$$\begin{aligned}\lim_{\varepsilon\to 0}\frac{L(\boldsymbol{\phi}(\Omega), \zeta(\boldsymbol{\phi}(\boldsymbol{x}))) - L(\Omega, \zeta(\boldsymbol{x}))}{\varepsilon} &= \dot{L}(\Omega, \zeta(\boldsymbol{x}), \boldsymbol{\varphi}) \\ &= \int_\Omega \{G'(\boldsymbol{x}, \zeta(\boldsymbol{x})) + \boldsymbol{\varphi}\cdot\nabla G(\boldsymbol{x}, \zeta(\boldsymbol{x})) + G(\boldsymbol{x}, \zeta(\boldsymbol{x}))\nabla\cdot\boldsymbol{\varphi}\}\, dx \\ &= \int_\Omega \{G'(\boldsymbol{x}, \zeta(\boldsymbol{x})) + \nabla\cdot(\boldsymbol{\varphi}G(\boldsymbol{x}, \zeta(\boldsymbol{x})))\}\, dx.\end{aligned} \tag{2.13}$$

Finally, based on the divergence theorem, we have

$$\dot{L}(\bar{\Omega}, \zeta(\boldsymbol{x}), \boldsymbol{\varphi}) = \int_\Omega G'(\boldsymbol{x}, \zeta(\boldsymbol{x}))\, dx + \int_{\partial\Omega} G(\boldsymbol{x}, \zeta)\boldsymbol{\nu}\cdot\boldsymbol{\varphi} d\gamma, \tag{2.14}$$

where $\dot{(\cdot)}$ and $(\cdot)'$ respectively represent the material derivative and the Fréchet derivative with respect to ζ, and where $\boldsymbol{\nu}$ denotes the outward unit normal vector on the boundary. Additional details about $\dot{(\cdot)}$ and $(\cdot)'$ are presented as Eqs. (15) and (16) of [18].

Considering the initial domain Ω and the design boundary $\partial\Omega_{\mathrm{m}}$, $\boldsymbol{\phi} = \mathbf{0}$ on $\partial\Omega_{\mathrm{m}}$, we have the first variation as

$$\dot{L}(\Omega \cup \partial\Omega_{\mathrm{m}}, \zeta(\boldsymbol{x}), \boldsymbol{\varphi}) = \int_\Omega G'(\boldsymbol{x}, \zeta(\boldsymbol{x}))\, dx + \int_{\partial\Omega_{\mathrm{m}}} G(\boldsymbol{x}, \zeta(\boldsymbol{x}))\boldsymbol{\nu}\cdot\boldsymbol{\varphi} d\gamma. \tag{2.15}$$

For sensitivity analysis, the adjoint variable method is used to derive a main problem and an adjoint problem by setting

$$\int_\Omega G'(\boldsymbol{x}, \zeta(\boldsymbol{x}))\, dx = 0. \tag{2.16}$$

After solving the main and the adjoint problems, the sensitivity is evaluated by substituting the main and adjoint variables into Eq. (2.15).

2.3 Main problems

For a shape optimization problem considering Snapshot POD, this paper presents the main problems: a non-stationary Navier–Stokes problem, and an eigenvalue problem in Snapshot POD. Below, the mapping $\boldsymbol{\phi}$ of the position vector $\boldsymbol{x}$ from the initial domain Ω to the optimal domain $\boldsymbol{\phi}(\Omega)$ is assumed as given. An initial domain Ω and the boundaries are found. Furthermore, the flow of a viscous incompressible fluid is assumed to occupy a bounded domain Ω in $\mathbb{R}^d$. The velocity $\boldsymbol{u}$ and pressure p are assumed to be satisfied in this domain Ω. The Reynolds number Re is defined with the reference length $|\Gamma_{\text{top}}|$ and the reference speed, which is the maximum value of the x-direction velocity component on Γ_{top}.

2.3.1 Non-stationary Navier–Stokes problem

Problem 1 (Non-stationary Navier–Stokes). *Find* $(\boldsymbol{u}, p) : \boldsymbol{\phi}(\Omega) \times (0, T) \to \mathbb{R}^d \times \mathbb{R}$ *such that*

$$\frac{D\boldsymbol{u}}{Dt} = -\nabla p + \frac{1}{\text{Re}}\,\Delta \boldsymbol{u} \quad \text{in } \boldsymbol{\phi}(\Omega) \times (0, T), \tag{2.17}$$

$$\nabla \cdot \boldsymbol{u} = 0 \quad \text{in } \boldsymbol{\phi}(\Omega) \times (0, T), \tag{2.18}$$

$$\boldsymbol{u} = \boldsymbol{u}_{\text{D}} \cos(2\pi t) \quad \text{on } \partial\Omega \times (0, T), \tag{2.19}$$

$$\boldsymbol{u} = \boldsymbol{u}^0 \quad \text{in } \boldsymbol{\phi}(\Omega) \text{ at } t = 0, \tag{2.20}$$

where

$$\boldsymbol{u}_{\text{D}} = \boldsymbol{0} \text{ on } \Gamma_{\text{wall}} \cup \boldsymbol{\phi}(\partial\Omega_{\text{m}}) \text{ and } \boldsymbol{u}_{\text{D}} = (16x^2(x-1)^2, 0) \text{ on } \Gamma_{\text{top}}, \tag{2.21}$$

and $\boldsymbol{u}^0$ represents a stationary solution of the stationary Navier–Stokes problem.

Letting $(\boldsymbol{w}, q)$ be adjoint variables with respect to the velocity and the pressure, then by discretizing in the time direction with the finite difference method, a set of necessary variables is found as $\zeta_1 = \{\boldsymbol{u}, p, \boldsymbol{w}, q\}$, where hereinafter $\boldsymbol{u} = \{\boldsymbol{u}^n\}_{n=N_1}^{N_2}$, $p = \{p^n\}_{n=N_1}^{N_2}$, $\boldsymbol{w} = \{\boldsymbol{w}^n\}_{n=N_1}^{N_2}$, and $q = \{q^n\}_{n=N_1}^{N_2}$. The variational form of the non-stationary Navier–Stokes problem is defined as

$$\begin{aligned} L_1(\Omega, \zeta_1) &= -\sum_{n=N_1}^{N_2} \left\{ \int_\Omega G_1^n(\boldsymbol{x}, \zeta_1)\, dx \right\} \\ &= 0, \ \forall (\boldsymbol{w}, q) \end{aligned} \tag{2.22}$$

by setting $m = N_2 - N_1 + 1$ with $N_1 = \frac{T_1}{\Delta t}$ and $N_2 = \frac{T_2}{\Delta t}$ for time step size Δt, at time $t = T_1, T_2$. The density function $G_1^n(\boldsymbol{x}, \zeta_1)$ is presented as

$$\begin{aligned} G_1^n(\boldsymbol{x}, \zeta_1) = &\frac{\boldsymbol{u}^{n+1}(\boldsymbol{x}) - \boldsymbol{u}^n(\boldsymbol{X}^n)}{\Delta t} \cdot \boldsymbol{w}^{n+1} \\ &- p^{n+1} \nabla \cdot \boldsymbol{w}^{n+1} - q^{n+1} \nabla \cdot \boldsymbol{u}^{n+1} + \frac{1}{\text{Re}} (\nabla \boldsymbol{u}^{n+1})^{\text{T}} : (\nabla \boldsymbol{w}^{n+1})^{\text{T}}, \end{aligned} \tag{2.23}$$

where $\boldsymbol{X}^n = \boldsymbol{x} - \Delta t \boldsymbol{u}^n$, using the characteristic finite element scheme presented by Notsu [20].

2.3.2 Snapshot Proper Orthogonal Decomposition

We define a Snapshot POD analysis from time $t = T_1$ to T_2, where a weight function is prepared to extract arbitrary primary components from all primary components.

The correlation coefficient matrix $\text{R} \in \mathbb{R}^{m \times m}$ is formed as

$$\tilde{\boldsymbol{u}} = [\boldsymbol{u}^{N_1}, \ldots, \boldsymbol{u}^{N_2}] \in \mathbb{R}^{d \times m} \tag{2.24}$$

as

$$\text{R}(N_1, N_2, \tilde{\boldsymbol{u}}, \tilde{\boldsymbol{u}}) = \int_\Omega \tilde{\boldsymbol{u}}^T \tilde{\boldsymbol{u}} dx.$$

Let eigenvalues and eigenvectors of R be $\omega \in \mathbb{R}^m$ and $\hat{\boldsymbol{u}} \in \mathbb{R}^{m \times m}$,

$$\begin{aligned} &\omega = [\omega^1, \ldots, \omega^i, \ldots, \omega^m], \ \omega^i \in \mathbb{R}, \\ &\hat{\boldsymbol{u}} = [\hat{\boldsymbol{u}}^1, \ldots, \hat{\boldsymbol{u}}^i, \ldots, \hat{\boldsymbol{u}}^m], \ \hat{\boldsymbol{u}}^i \in \mathbb{R}^m, \\ &\boldsymbol{\Phi} = \tilde{\boldsymbol{u}} \hat{\boldsymbol{u}} \omega^{-\frac{1}{2}} \in \mathbb{R}^{d \times m}, \\ &\boldsymbol{\omega}^{-\frac{1}{2}} = \text{diag}(\omega_i^{-\frac{1}{2}})_i \end{aligned}$$

where $\text{R}(N_1, N_2, \tilde{\boldsymbol{u}}, \tilde{\boldsymbol{u}})$ is a positive-semidefinite matrix satisfying the eigenvalue $0 \le \omega$, and where $\boldsymbol{\Phi}^i$ represents the POD basis for the i-th primary component as

$$\boldsymbol{\Phi} = [\boldsymbol{\Phi}^1, \ldots, \boldsymbol{\Phi}^i, \ldots, \boldsymbol{\Phi}^m] \in \mathbb{R}^{d\times m}.$$

Using the definitions, we define snapshot POD analysis as described below.

Problem 2 (Snapshot Proper Orthogonal Decomposition)**.** *Let the solution* $\boldsymbol{u}$ *of Problem 1 be given. Find* $\omega \in \mathbb{R}^m$ *and* $\hat{\boldsymbol{u}} \in \mathbb{R}^{m\times m}$ *for* $N_1, N_2 \in \mathbb{N}$ *such that*

$$\operatorname{diag}\omega\hat{\boldsymbol{u}} - \mathrm{R}(N_1, N_2, \tilde{\boldsymbol{u}}, \tilde{\boldsymbol{u}})\hat{\boldsymbol{u}} = 0. \tag{2.25}$$

For the optimization problem, let $\zeta_2 = \{\omega, \hat{\boldsymbol{u}}, \boldsymbol{\alpha}, \boldsymbol{u}\}$ be the set of necessary variables used in Problem 2, where $\boldsymbol{\alpha}$ is an adjoint variable for the eigenvectors $\hat{\boldsymbol{u}}$.

$$\boldsymbol{\alpha} = [\boldsymbol{\alpha}^1, \ldots, \boldsymbol{\alpha}^i, \ldots, \boldsymbol{\alpha}^m],\ \boldsymbol{\alpha}^i \in \mathbb{R}^m. \tag{2.26}$$

For the shape optimization problem studied here, Snapshot POD is a main problem. It plays a role as one of a constration function. Therefore, the following functional is defined as

$$L_2(\Omega, \zeta_2) = -G_2(\boldsymbol{x}, \zeta_2), \tag{2.27}$$

where

$$G_2(\boldsymbol{x}, \zeta_2) = \boldsymbol{\alpha} \cdot [\delta_{j\to k}\{\operatorname{diag}\omega\hat{\boldsymbol{u}} - \mathrm{R}\hat{\boldsymbol{u}}\}], \tag{2.28}$$

where $\delta_{j\to k}$ represents the weight function used to extract j to the k primary components in 1 to the m primary components.

$$\delta_{j\to k} = \operatorname{diag}(0, \ldots, 0, \overset{j}{1}, \ldots, \overset{k}{1}, 0, \ldots, 0)$$

3. Shape Optimization Problem

The shape optimization problem using Snapshot POD with the weight function $\delta_{j\to k}$ is constructed next, with the Lagrange function first defined to deduce the first variation. Next, based on the Kuhn–Tucker condition, the main and adjoint problems are solved to obtain the main and adjoint variables, which are substituted into the first variation to evaluate sensitivity for the shape optimization problem as summarized in Sect. 2.2.

3.1 Lagrange function and its material derivative

We formulate the following minimization problem of the cost function f as

$$f(\omega) = \sum_{i=N_1}^{N_2} \delta_{j\to k}\omega_i, \tag{3.1}$$

where $\delta_{j\to k}$ represents the weight function introduced into Sect. 2.3.2.

Problem 3 (Shape Optimization)**.** *After letting* $f(\omega)$ *be defined as Eq. (3.1), we find* $\boldsymbol{\phi}(\Omega)$ *such that*

$$\min_{\boldsymbol{\phi}}\{f(\omega);\ \{(\boldsymbol{u}^n, p^n)\}_{n=N_1}^{N_2},\ (\omega, \hat{\boldsymbol{u}})\}. \tag{3.2}$$

By application of the Lagrange multiplier method, Lagrange function L for the shape optimization problem in this study can be expressed as

$$L(\Omega, \zeta_1, \zeta_2) = f(\omega) + L_1(\Omega, \zeta_1) + L_2(\Omega, \zeta_2). \tag{3.3}$$

3.2 Main and adjoint problems

Based on the adjoint variable method, the main problems of Problem 3 are introduced into Problem 1 and Problem 2. Also, the adjoint problems of Problem 3 are given as presented below.

Problem 4 (Adjoint Problem for $\boldsymbol{\alpha}$)**.** *Given eigenfunction* $\hat{\boldsymbol{u}}$ *of Problem 2, then find* $\boldsymbol{\alpha} \in \mathbb{R}^{m\times m}$ *such that*

$$\hat{\boldsymbol{u}}\boldsymbol{\alpha} = \boldsymbol{I}, \tag{3.4}$$

and $\hat{\boldsymbol{u}}, \boldsymbol{\alpha}$ *are the unitary matrix from Problem 4. Therefore,* $\boldsymbol{\alpha}$ *is obtained as the inverse matrix or the transposed matrix of* $\hat{\boldsymbol{u}}$*:*

$$\boldsymbol{\alpha} = \hat{\boldsymbol{u}}^{-1} = \hat{\boldsymbol{u}}^{\mathrm{T}}. \tag{3.5}$$

Problem 5 (Adjoint Problem for $\boldsymbol{\alpha}$)**.** *Let the solution* $\boldsymbol{u}$ *of Problem 1 be given. Find* $\boldsymbol{\alpha}^{\mathrm{T}} \in \mathbb{R}^{m\times m}$ *such that*

$$\operatorname{diag} \omega \boldsymbol{\alpha}^{\mathrm{T}} = \mathrm{R}(N_1, N_2, \tilde{\boldsymbol{u}}, \tilde{\boldsymbol{u}})\boldsymbol{\alpha}^{\mathrm{T}}. \tag{3.6}$$

In fact, solving Problem 5 is unnecessary because $\boldsymbol{\alpha}$ *has already been obtained in Problem 4.*

Problem 6 (Adjoint Problem for $(\bar{\boldsymbol{u}}, \bar{p})$)**.** *With* $\boldsymbol{\phi}$ *and the time-averaged solution* $(\bar{\boldsymbol{u}}, \bar{p})$ *of Problem 1, and with the eigenvalue and the eigenfunction* $(\omega, \hat{\boldsymbol{u}})$ *of Problem 2 with* $\hat{\boldsymbol{u}} = \boldsymbol{\alpha}^{\mathrm{T}}$ *as given, find* $(\bar{\boldsymbol{w}}, \bar{q}) : \Omega \to \mathbb{R}^d \times \mathbb{R}$ *such that*

$$(\nabla \bar{\boldsymbol{u}}^{\mathrm{T}})\bar{\boldsymbol{w}} - (\bar{\boldsymbol{u}} \cdot \nabla)\bar{\boldsymbol{w}} + \nabla \bar{q} - \frac{1}{\mathrm{Re}} \Delta \bar{\boldsymbol{w}} + \bar{\boldsymbol{A}} = \boldsymbol{0} \text{ in } \Omega, \tag{3.7}$$

$$\nabla \cdot \bar{\boldsymbol{w}} = \boldsymbol{0} \text{ in } \Omega, \tag{3.8}$$

$$\bar{\boldsymbol{w}} = \boldsymbol{0} \text{ on } \partial\Omega, \tag{3.9}$$

where

$$\bar{\boldsymbol{A}} = 2 \sum_{i=N_1}^{N_2} \delta_{j \to k} \boldsymbol{\alpha} \boldsymbol{\Phi}_{\omega}^{\mathrm{T}}, \quad \bar{\boldsymbol{u}} = \sum_{n=N_1}^{N_2} \boldsymbol{u}^n, \quad \boldsymbol{\Phi}_{\omega} = \boldsymbol{\Phi} \omega^{-\frac{1}{2}}. \tag{3.10}$$

3.3 Sensitivity of the shape optimization problem

Here, based on the adjoint variable method, we evaluate the sensitivity of the shape optimization problem on the design boundary $\partial\Omega_{\mathrm{m}}$, as

$$\bar{G_1}(\boldsymbol{x}, \zeta_1(\Omega)) = -\frac{1}{\mathrm{Re}} \nabla \bar{\boldsymbol{u}}^{\mathrm{T}} : \nabla \bar{\boldsymbol{w}}^{\mathrm{T}}.$$

4. Adaptive Mesh Refinement

In this section, AMR distributed in Freefem++ [19] is summarized as explained below.

Letting $\eta(\boldsymbol{x})$ be a data function describing any physical state in the domain for finite element method, then a Taylor expansion of the data function $\eta(\boldsymbol{x})$ with respect to any interior point $\boldsymbol{x}$ in an element over a mesh can be expressed as

$$\begin{aligned} \eta(\boldsymbol{x}) &= \eta(\boldsymbol{x}_c + t\boldsymbol{\delta x}) \\ &= \eta(\boldsymbol{x}_c) + \{(\nabla \eta)|_{\boldsymbol{x}=\boldsymbol{x}_c}\}^{\mathrm{T}}(t\boldsymbol{\delta x}) + \frac{1}{2}(t\boldsymbol{\delta x})^{\mathrm{T}}\{(\nabla\nabla\eta)|_{\boldsymbol{x}=\boldsymbol{x}_c}\}(t\boldsymbol{\delta x}) + o((\boldsymbol{\delta x})^3) \\ &= \eta_h(\boldsymbol{x}) + \frac{1}{2}(t\boldsymbol{\delta x})^{\mathrm{T}}\{(\nabla\nabla\eta)|_{\boldsymbol{x}=\boldsymbol{x}_c}\}(t\boldsymbol{\delta x}) + o((\boldsymbol{\delta x})^3), \end{aligned} \tag{4.1}$$

for $t \in [0, 1]$, where $\boldsymbol{x}_c$ represents the position vector at a node of an element in a mesh, and where η_h denotes the linear approximation for η. The interpolation error $e(\boldsymbol{x})$ at a displacement $t\boldsymbol{\delta x}$ from node $\boldsymbol{x}_c$ can be expressed as

$$\begin{aligned} e(\boldsymbol{x}) &= \left| \int_0^1 \{\eta(\boldsymbol{x}) - \eta_h(\boldsymbol{x})\} dt \right| \\ &\approx \left| \int_0^1 \left[\frac{1}{2}(t\boldsymbol{\delta x})^{\mathrm{T}}\{(\nabla\nabla\eta)|_{\boldsymbol{x}=\boldsymbol{x}_c}\}(t\boldsymbol{\delta x}) \right] dt \right| \\ &\le \frac{1}{2}(\boldsymbol{\delta x})^{\mathrm{T}} |\nabla\nabla\eta|_{\boldsymbol{x}=\boldsymbol{x}_c} (\boldsymbol{\delta x}) \int_0^1 t^2 dt \\ &= \frac{1}{6}(\boldsymbol{\delta x})^{\mathrm{T}} |\nabla\nabla\eta|_{\boldsymbol{x}=\boldsymbol{x}_c} (\boldsymbol{\delta x}) \end{aligned} \tag{4.2}$$

As described herein, after the domain is reshaped every reshaping step, an isotropic meshing is regarded as maintaining the same numerical accuracy as the initial domain over the mesh throughout this optimization process. Therefore, the Hessian matrix $\nabla\nabla\eta$ is the identity matrix for the case in which $\eta = \frac{1}{2}(\boldsymbol{\delta x})^{\mathrm{T}}(\boldsymbol{\delta x})$ is used. Finally, the maximal interpolation error over a mesh is written as

$$e(\boldsymbol{x}) = \frac{1}{6} h_{\max}^2, \tag{4.3}$$

where $h_{\max}$ represents the maximal length for all edges. The author only works with one variable η for meeting the fixed error tolerance ε_h that must be equidistributed over the mesh as

$$\sup_{\boldsymbol{x} \in \boldsymbol{\phi}(\Omega)} |\eta(\boldsymbol{x}) - \eta_h(\boldsymbol{x})| \le \frac{1}{6} \varepsilon_h. \tag{4.4}$$

The procedure of AMR distributed in Freefem++ is the following for $i = 1 \cdots N_{\mathrm{nodes}}$, where $N_{\mathrm{nodes}} \in \mathbb{N}$ represents the number of the nodes.

Step 1 Set $i = 1$ and ε_h arbitrarily.
Step 2 Let d_i stand for the length of the edge a_i.
Step 3 Compare ε_h and d_i:
- If $d_i > \varepsilon_h$ and $i \leq N_{\text{nodes}}$, then the edge a_i must be cut into two edge and return to Step 2.
- If $d_i \leq \varepsilon_h$ and $i \leq N_{\text{nodes}}$, then replace i with $i + 1$ and return to Step 2.
- Otherwise stop.

Additional details related to the numerical procedure are reported elsewhere in the literature [11] along with a mathematical proof in continuous and discrete spaces of the domain [12].

5. Numerical Schemes

The Taylor–Hood (P2-P1) element pair for the velocity and pressure is used to discretize all equations spatially. FreeFEM++ [19] is used for all numerical calculations.

The stationary solution $(\boldsymbol{u}^0, p^0)$ is obtained to solve the stationary Navier–Stokes problem using the Newton–Raphson method. The non-stationary solution $\{(\boldsymbol{u}^n, p^n)\}_{n=1}^N$ is obtained to solve Problem 1 with the UMFPACK solver presented in [21] for every time step from $n = 1$ to N. For the material derivative term, the characteristic curve method is used. Using it, Notsu and Tabata [20] proved its mathematical proof and numerical availability. The solver for the characteristic curve method is distributed in Freefem++ [19]. After obtaining the non-stationary solution $\{(\boldsymbol{u}^n, p^n)\}_{n=1}^N$, the correlation coefficient matrix R is formed for snapshot POD. The eigenvalue problem for the matrix R is solved in Problem 2 using lapack solver.

Based on the theory of the optimization problem considered herein, the adjoint problem of Problem 6 is solved to obtain $(\bar{\boldsymbol{w}}, \bar{q})$ with UMFPACK solver [21]. After evaluating the sensitivity, for domain deformation, the H^1 gradient method is used with UMFPACK solver [21]. Finally, AMR is applied after moving meshes every reshaping step, where the adaptive mesh solver is distributed in Freefem++, as discussed in [19].

6. Numerical Calculations and Discussion

In this section, some parameters for numerical calculations are decided in Sect. 6.1. Numerical calculation results are discussed in Sect. 6.2.

6.1 Spatial and temporal discretization, adaptive mesh refinement

For comparisons with numerical calculations in [1], the same numerical accuracy evaluation is used as explained below. Velocity and pressure are discretized in the spatial direction using finite element method, with respective nodes and elements of $(N_{\text{nodes}}, N_{\text{elements}}) = (21945, 43290)$. For discretization in time, the time step size $\Delta t = 0.001$ is used to take time integrations of Problem 1 at $\text{Re} = 100$. Velocity vectors are sampled from $T_1 = 3$ to $T_2 = 6$ for Snapshot POD. Additional details of numerical accuracy are presented in Appendix A of an earlier report [1].

For AMR in the case of $\eta = \frac{1}{2}\boldsymbol{x}^{\mathrm{T}}\boldsymbol{x}$, the maximum interpolation error $e(\boldsymbol{x})$ in triangles over mesh is evaluated with the longest edge length $h_{\max}$ in the initial mesh. From the discussion presented in Sect. 4, the interpolation error is satisfied throughout the shape optimization process.

6.2 Numerical results

As explained in this subsection, the three cases of $\delta_{1\to1}$ and $\delta_{1\to4}$ and $\delta_{2\to4}$ are regarded as a better combination of eigenvalues in Snapshot POD. In fact, in the domain of interest, the power spectral density from the first to the fourth primary components was reported as higher than 99% [1]. Therefore this discussion addresses only the primary components up to the fourth.

The optimal meshes with and without AMR are presented in Fig. 1 for $\delta_{1\to1}$ and Fig. 2 for $\delta_{1\to4}$ and Fig. 3 for $\delta_{2\to4}$. As these figures show, AMR apparently accommodates more complex domain deformation than the case without AMR, especially on and near the boundary with high curvature. The POD basis is shown in Appendix A.

Next, values of the cost functions are compared for three cases of eigenvalue combinations. Normalized cost functions f^k/f^0 for $\delta_{1\to1}$ and $\delta_{1\to4}$ and $\delta_{2\to4}$ are presented in Figs. 4, 5, and 6. Apparently, the cost function with AMR can converge to a greater degree than without AMR throughout the shape-reshaping step.

Finally, we show eigenvalues ω_1 and $\sum_{i=2}^4 \omega_i$ in the initial and the optimal domains with AMR in Tables 1 and 2, and 3 for three cases. Subsequently, we discuss efficiencies to suppress the time periodic flow. In fact, the first primary component eigenvalue ω_1 and the eigenvalues over the second primary component $\sum_{i=2}^4 \omega_i$ represent the L^2 norm of the time average velocity and the time fluctuation velocity vectors obtained by decomposing the time periodic flow into primary components. Results clarify that the case of $\delta_{2\to4}$ decreases $\sum_{i=2}^4 \omega_i$ more than any other case. This result suggests that $\delta_{2\to4}$ can best suppress the amplitude of the time periodic flows.

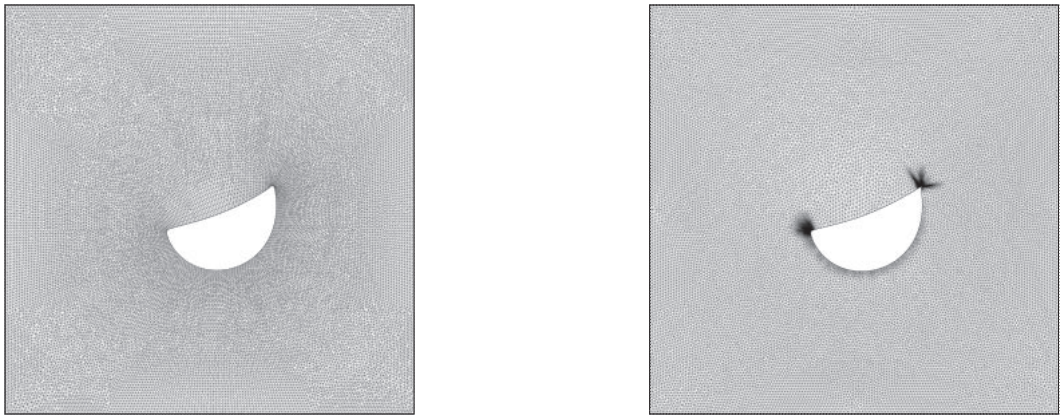

(a) Without AMR (b) With AMR

Fig. 1. For $\delta_{1\to1}$, optimal meshes (a) without and (b) with AMR.

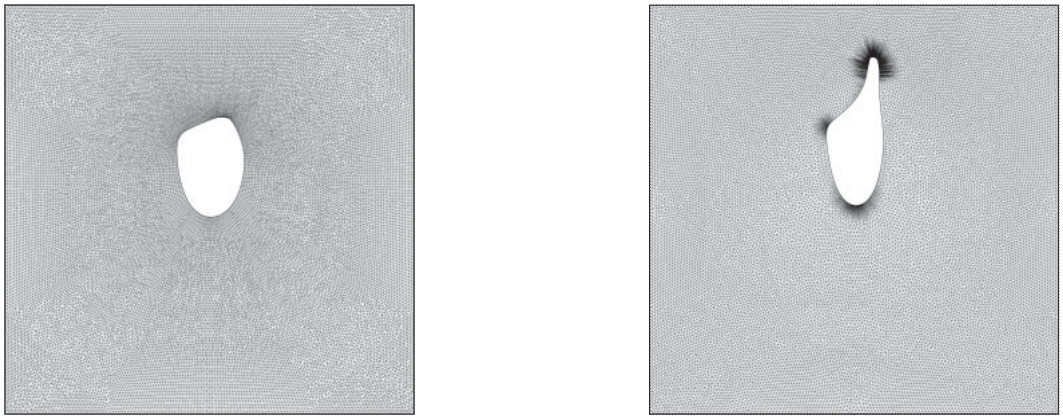

(a) Without AMR (b) With AMR

Fig. 2. For $\delta_{1\to4}$, optimal meshes (a) without and (b) with AMR.

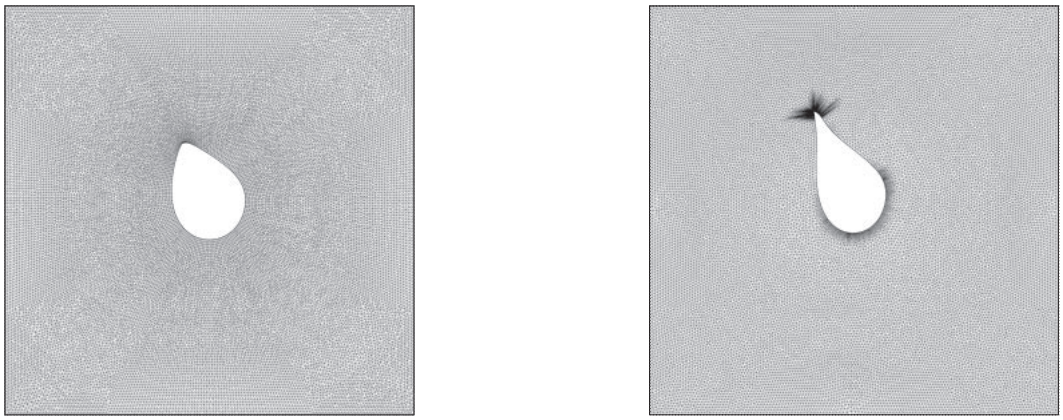

(a) Without AMR (b) With AMR

Fig. 3. For $\delta_{2\to4}$, optimal meshes (a) without and (b) with AMR.

7. Conclusions

As described herein, the author combines AMR with a shape optimization method for suppressing moderate time periodic flow fields at a sufficiently low Reynolds number considering Snapshot POD formulated in [1]. Particularly, the sum of eigenvalues in Snapshot POD is defined as the cost function. The non-stationary Navier–Stokes problem and the eigenvalue problem in Snapshot POD are used as main problems. The main problems are transformed from strong forms to weak forms with trial functions based on a standard framework of the finite element method (FEM). The

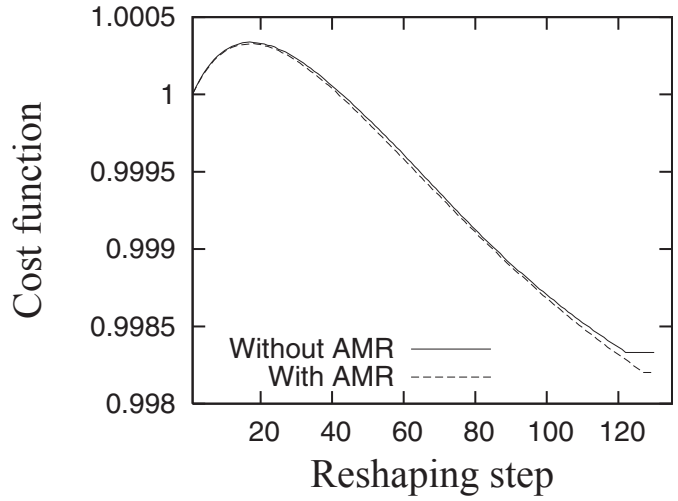

Fig. 4. For $\delta_{1\to1}$, normalized cost functions f^k/f^0 with reshaping step $k = 135$ at $\mathrm{Re} = 100$.

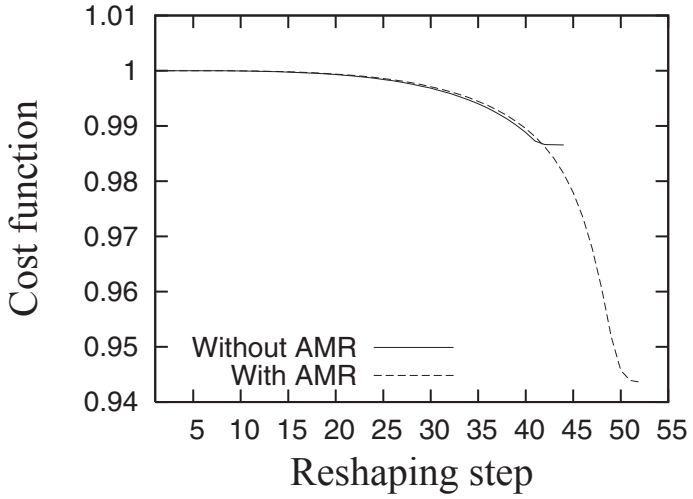

Fig. 5. For $\delta_{1\to4}$, normalized cost functions f^k/f^0 with reshaping step $k = 55$ at $\mathrm{Re} = 100$.

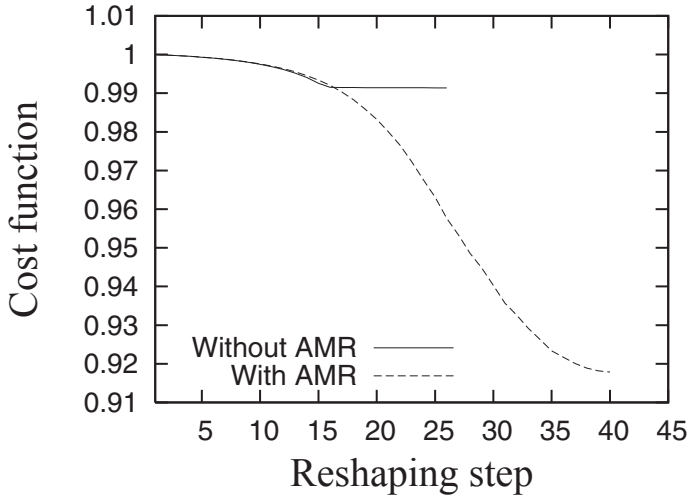

Fig. 6. For $\delta_{2\to4}$, the normalized cost function f^k/f^0 with reshaping step $k = 45$ at $\mathrm{Re} = 100$.

functional is described using the Lagrange multiplier method with FEM. Next, its material derivative is derived to evaluate the sensitivity using adjoint variable method. The initial domain is reshaped iteratively until the cost function satisfies the terminal condition, where the H^1 gradient method is used for stable domain deformation. This study uses AMR. Every mesh is reshaped by sensitivity, where the new mesh is generated in the case of $\eta = \frac{1}{2}\boldsymbol{x}^{\mathrm{T}}\boldsymbol{x}$ and the

Table 1. For $\delta_{1\to1}$, eigenvalues ω_1 and $\sum_{i=2}^{4}\omega_i$ in the initial and optimal domains with AMR.

ω_i	Ω	$\boldsymbol{\phi}(\Omega)$ with AMR
ω_1	0.15180	0.15181
$\sum_{i=2}^{4}\omega_i$	0.02931	0.02930

Table 2. For $\delta_{1\to4}$, eigenvalues ω_1 and $\sum_{i=2}^{4}\omega_i$ in the initial and optimal domains with AMR.

ω_i	Ω	$\boldsymbol{\phi}(\Omega)$ with AMR
ω_1	0.15184	0.14410
$\sum_{i=2}^{4}\omega_i$	0.02931	0.02930

Table 3. For $\delta_{2\to4}$, eigenvalues ω_1 and $\sum_{i=2}^{4}\omega_i$ in the initial and optimal domains with AMR.

ω_i	Ω	$\boldsymbol{\phi}(\Omega)$ with AMR
ω_1	0.15202	0.150981
$\sum_{i=2}^{4}\omega_i$	0.0285624359	0.0247816991

maximum interpolation error $e(\boldsymbol{x})$ in triangles over mesh is evaluated with the longest edge length $h_{\max}$ in the initial mesh. Thereby, based on a discussion of Sect. 4, the interpolation error is satisfied throughout the shape optimization process. A two-dimensional cavity flow with a disk-shaped isolated body is used for a numerical demonstration. Numerical results reveal that the optimal domain with AMR can decrease the L^2 norm of the time average and that the time fluctuation affects flow fields ω_1 and $\sum_{i=2}^{4}\omega_i$, to a greater degree than in the initial domain. Suppressing time-dependent flow efficiently requires that one ascertain a combination of the eigenvalues (POD modes) to decrease the L^2 norm of the time fluctuation velocity vector $\sum_{i=2}^{4}\omega_i$.

Appendix: POD Basis

Figures A·1–A·7 are stream functions of POD basis $\boldsymbol{\Phi}^i$ at the i primary components of $i = 1$–4.

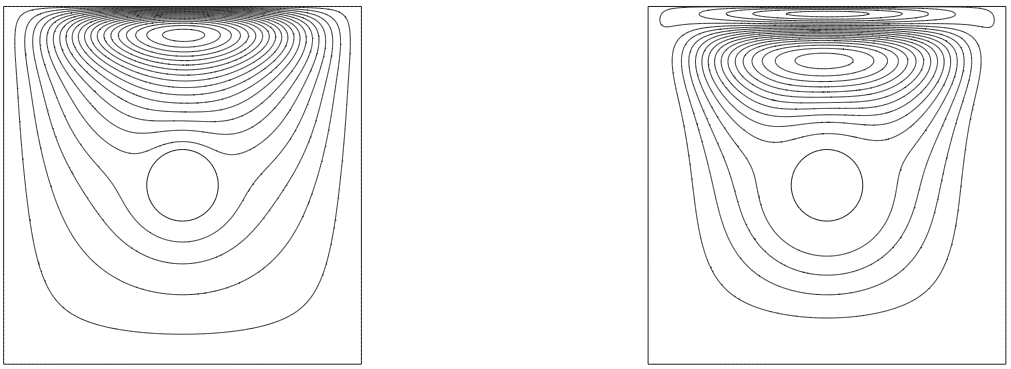

(a) $i = 1$ (b) $i = 2$

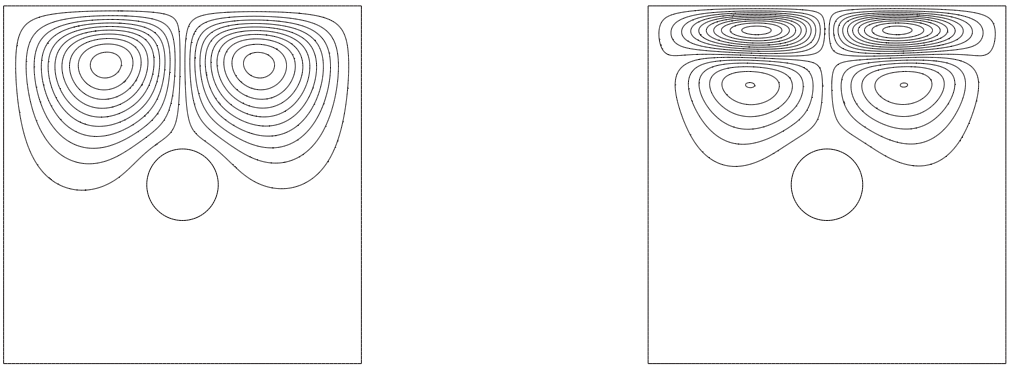

(a) $i = 3$ (b) $i = 4$

Fig. A·1. Stream functions of POD basis at the i-th primary components from $i = 1$ to 4 at Re = 100 in the initial domain Ω.

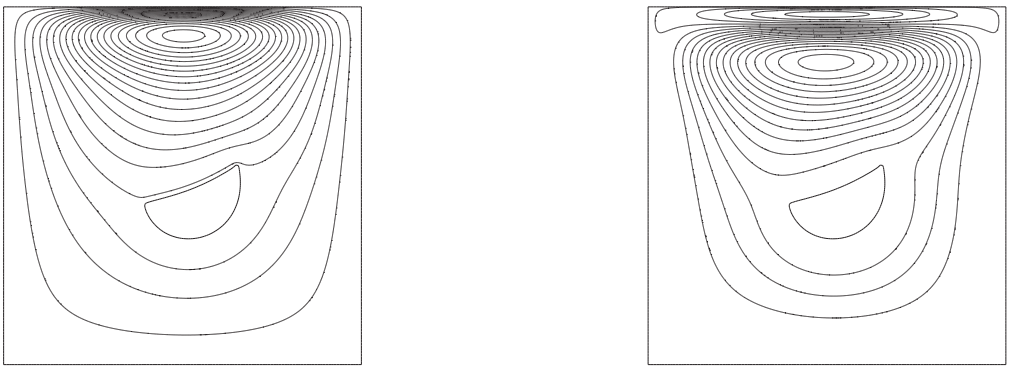

(a) $i = 1$ (b) $i = 2$

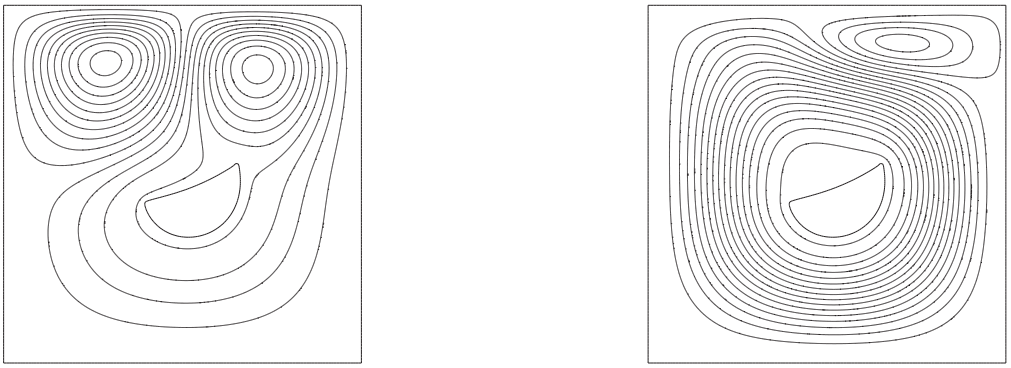

(a) $i = 3$ (b) $i = 4$

Fig. A·2. For $\delta_{1\to 1}$, stream functions of the POD basis at the i-th primary components from $i = 1$ to 4 at $\mathrm{Re} = 100$ in the optimal domain $\boldsymbol{\phi}(\Omega)$ without AMR.

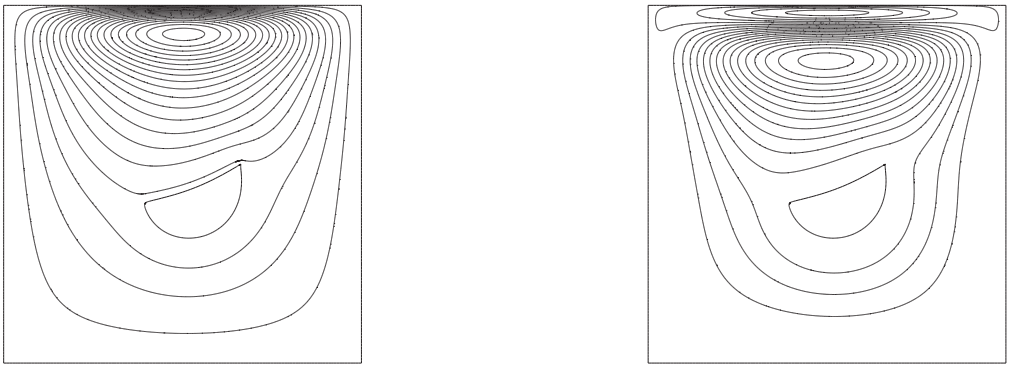

(a) $i = 1$ (b) $i = 2$

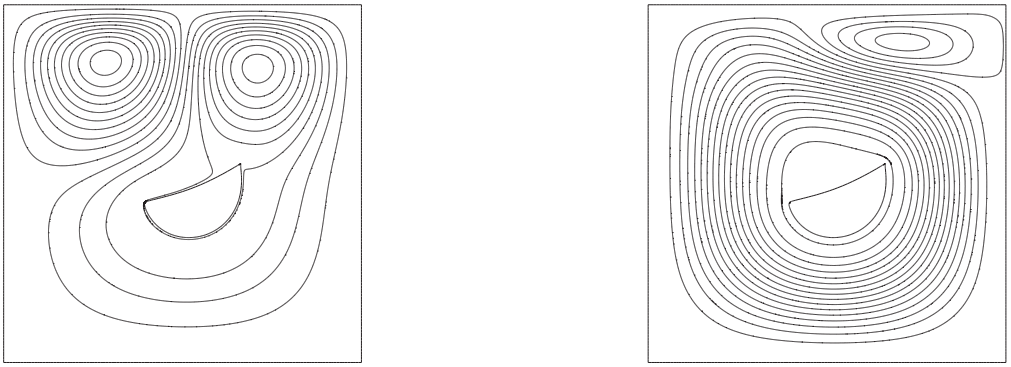

(a) $i = 3$ (b) $i = 4$

Fig. A·3. For $\delta_{1\to 1}$, stream functions of POD basis at the i-th primary components from $i = 1$ to 4 at $\mathrm{Re} = 100$ in the optimal domain $\boldsymbol{\phi}(\Omega)$ with AMR.

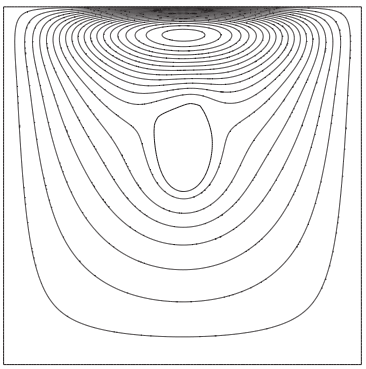

(a) $i = 1$

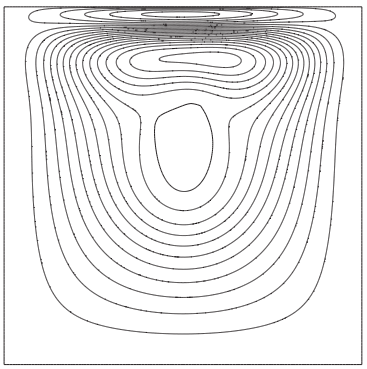

(b) $i = 2$

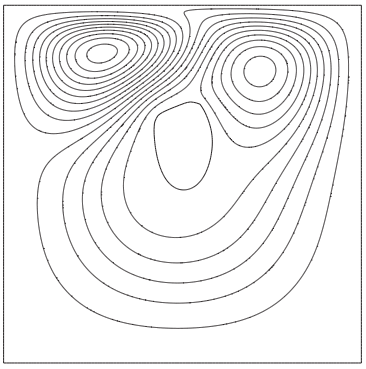

(a) $i = 3$

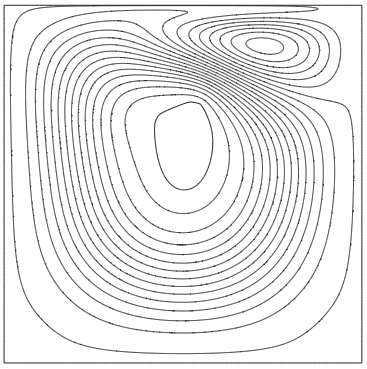

(b) $i = 4$

Fig. A·4. For $\delta_{1\to4}$, stream functions of POD basis at the i-th primary components from $i = 1$ to 4 at $\mathrm{Re} = 100$ in the optimal domain $\boldsymbol{\phi}(\Omega)$ without AMR.

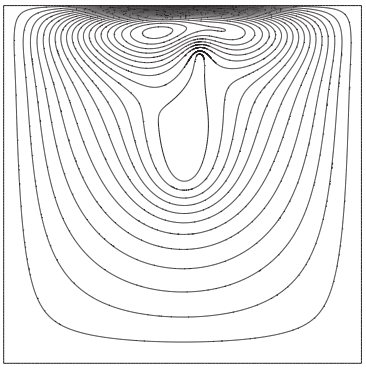

(a) $i = 1$

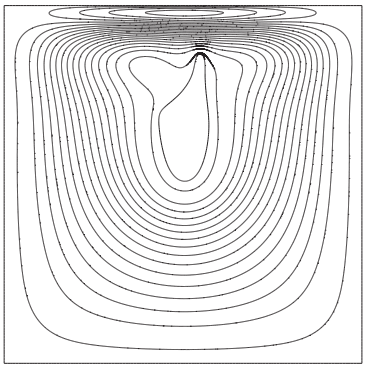

(b) $i = 2$

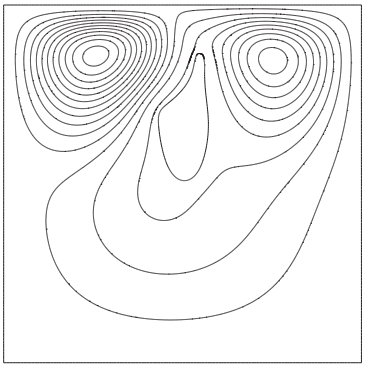

(a) $i = 3$

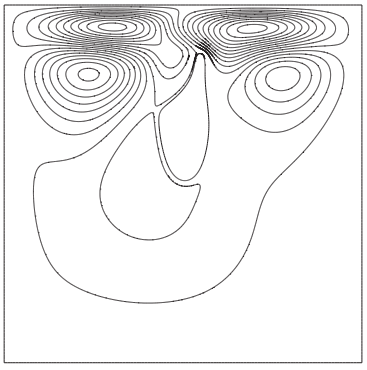

(b) $i = 4$

Fig. A·5. For $\delta_{1\to4}$, stream functions of POD basis at the i-th primary components from $i = 1$ to 4 at $\mathrm{Re} = 100$ in the optimal domain $\boldsymbol{\phi}(\Omega)$ with AMR.

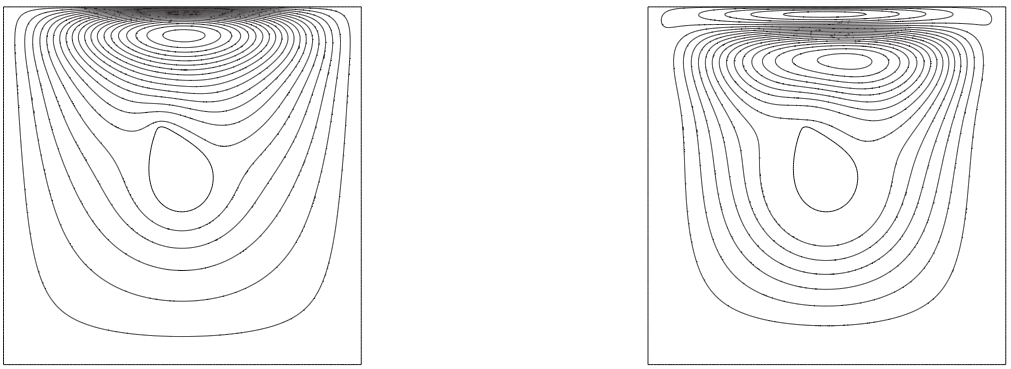

(a) $i = 1$ (b) $i = 2$

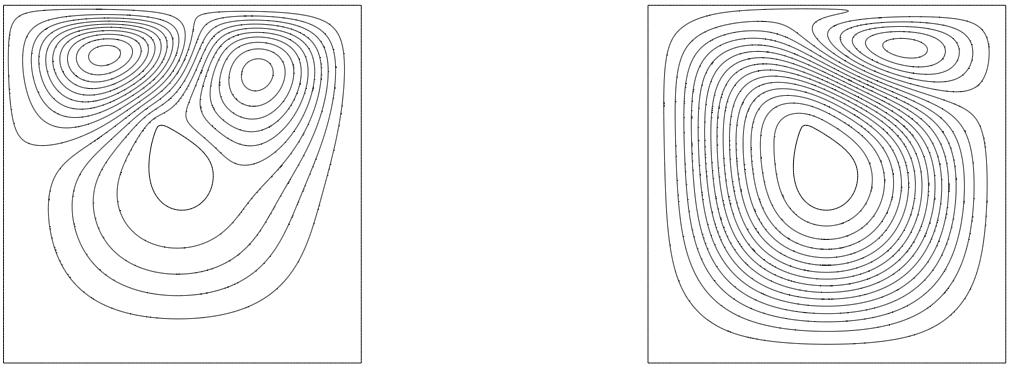

(a) $i = 3$ (b) $i = 4$

Fig. A·6. For $\delta_{2\to4}$, stream functions of POD basis at the i-th primary components from $i = 1$ to 4 at $\mathrm{Re} = 100$ in the optimal domain $\boldsymbol{\phi}(\Omega)$ without AMR.

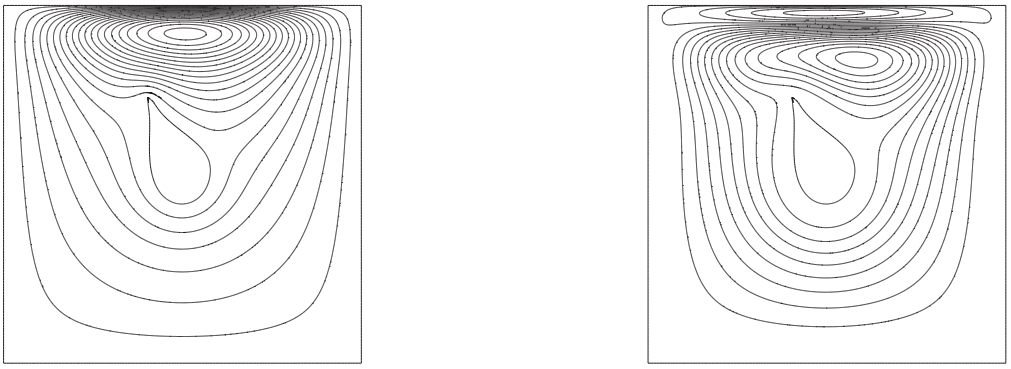

(a) $i = 1$ (b) $i = 2$

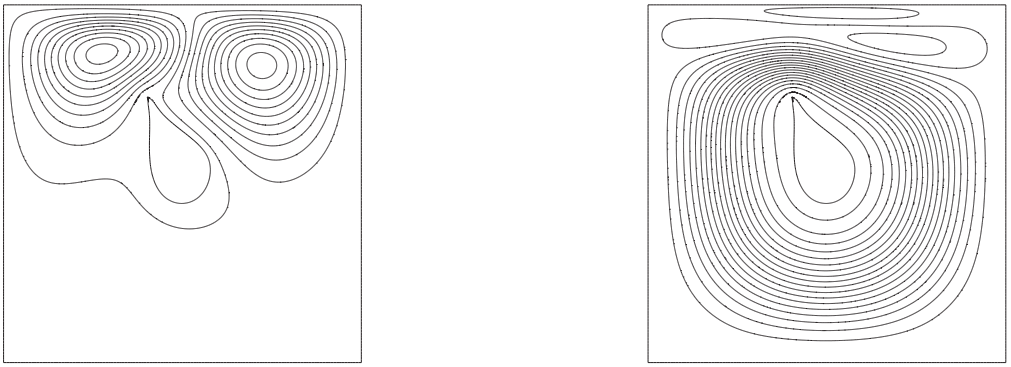

(a) $i = 3$ (b) $i = 4$

Fig. A·7. For $\delta_{2\to4}$, stream functions of POD basis at the i-th primary components from $i = 1$ to 4 at $\mathrm{Re} = 100$ in the optimal domain $\boldsymbol{\phi}(\Omega)$ with AMR.

REFERENCES

[1] Nakazawa, T., "Shape optimization of flow fields considering proper orthogonal decomposition," *Math. Anal. Cont. Mech. Indust. Appl.*, **3** (2018).
[2] Pironneau, O., "On optimum profiles in Stokes flow," *JFM*, **59**: 117–128 (1973).
[3] Pironneau, O., "On optimum design in fluid mechanics," *JFM*, **64**: 97–110 (1974).
[4] Haslinger, J., and Makinen, A. E., Introduction to Shape Optimization: Theory, Approximation, and Computation, SIAM, Philadelphia (2003).
[5] Mohammadi, B., and Pironneau, O., Applied Shape Optimization for Fluids, Oxford University Press (2001).
[6] Moubachir, M., and Zolesio, J. P., Moving Shape Analysis and Control: Applications to Fluid Structure Interactions, Chapman and Hall/CRC Pure and Applied Mathematics, Boca Raton (2006).
[7] Shinohara, K., Okuda, H., Ito, S., Nakajima, N., and Ida, M., "Shape optimization using adjoint variable method for reducing drag in Stokes flow," *Int. J. Numer. Meth. Fluids*, **58**: 119–159 (2008).
[8] Katamine, E., Nagatomo, Y., and Azegami, H., "Shape optimization of 3D viscous flow fields," *Inverse Prob. Sci. Eng.*, **17**: 105–114 (2009).
[9] Ghosh, S., Pratihar, D. K., Maiti, B., and Das, P. K., "An evolutionary optimization of diffuser shapes based on CFD simulations," *Int. J. Numer. Meth. Fluids*, **63**: 1147–1166 (2010).
[10] Iwata, Y., Azegami, H., and Katamine, E., "Numerical Solution to shape optimization problem for non-stationary Navier–Stokes problems," *JSIAM Letters*, **2**: 37–40 (2010).
[11] Castro-Diaz, M. J., and Hecht, F., "Anisotropic surface mesh generation," *INRIA Res. Rep.*, **2672**: 1–31 (2006).
[12] Alauzet, F., Loseille, A., Dervieux, A., and Frey, J. P., Multi-dimensional Continuous Metric for Mesh Adaptation, In Proc. of 15th Int. Meshing Roundtable, Vol. 15, pp. 191–214 (2006).
[13] Castro-Diaz, M. J., Hecht, F., Mohammadi, B., and Pironneau, O., "Anisotropic unstructured mesh adaptation for flow simulations," *Int. J. Numer. Meth. Fluids*, **25**: 475–491 (1997).
[14] Mohammadi, B., and Hecht, F., "Mesh adaptation for time dependent simulation, optimization and control," *Revue Europeenne deselements finis*, **10**: 575–595 (2001).
[15] Frey, J. P., and Alauzet, F., Anisotropic Mesh Adaptation for Transient Flows Simulations, In Proc. of 12th Int. Meshing Roundtable, Vol. 12, pp. 335–348 (2003).
[16] Nakazawa, T., Increasing the Critical Reynolds Number by Maximizing Dissipation Energy Problem, Proceedings of the Fifth International Conference on Jets, Wakes and Separated Flows (ICJWSF2015), Ed. Segalini, A., Chapter 75, pp. 613–620 (2016).
[17] Nakazawa, T., and Azegami, H., "Shape optimization method improving hydrodynamic stability," *Jpn. J. Indust. Appl. Math.*, **33**: 167–181 (2015).
[18] Azegami, H., and Wu, Z., "Domain optimization analysis in linear elastic problems: Approach using traction method," *JSME Int. J. Ser. A*, **39**: 272–278 (1996).
[19] Hecht, F., "New development in FreeFem++," *J. Numerical Math.*, **20**: 251–265 (2012).
[20] Notsu, H., and Tabata, M., "Error estimates of a pressure-stabilized characteristics finite element scheme for Oseen equations," *J. Sci. Comput.*, **65**: 940–955 (2015).
[21] Davis, T., "Algorithm 832: UMFPACK, an unsymmetric-pattern multifrontal method," *ACM Trans. Math. Software*, **30**: 196–199 (2004).